Euro. Jnl of Applied Mathematics (2008), *vol.* 19, *pp.* 311–327.
doi:10.1017/S0956792508007390 Printed in the United Kingdom

A numerical method for coupled surface and grain boundary motion

ZHENGUO PAN[1] and BRIAN WETTON[2]

[1]*Department of Mathematics, University of British Columbia, Vancouver, B.C. Canada V6T 1Z*
email: panzg@math.ubc.ca
[2]*Department of Mathematics, University of British Columbia, Vancouver, B.C. Canada V6T 1Z2*
email: wetton@math.ubc.ca

(*Received 8 March 2007; revised 25 February 2008*)

We study the coupled surface and grain boundary motion in a bi-crystal in the context of the 'quarter loop' geometry. Two types of normal curve velocities are involved in this model: motion by mean curvature and motion by surface diffusion. Three curves meet at points where junction conditions are given. A formulation that describes the coupled normal motion of the curves and preserves arc length parametrisation up to scaling is proposed. The formulation is shown to be well-posed in a simple, linear setting. Equations and junction conditions are approximated by finite difference methods. Numerical convergence to exact travelling wave solutions is shown. The method is applied to other problems of physical interest.

1 Introduction

Coupled surface and grain boundary motion is an important phenomenon controlling the grain growth in materials processing and synthesis. A commonly used model to study this coupled effect is called 'quarter loop' geometry introduced by Dunn *et al.* [11].

In the quarter loop geometry, there are two crystal grains between which there is an interface called grain boundary as shown in Figure 1. The two grains are of the same material and differ only in their relative crystalline orientation. The grain boundary runs parallel to a free surface before it turns up and attaches to upper surfaces at the groove root. When heated at a specific temperature, the grain boundary migrates to reduce the surface energy and to heal the orientation mismatch. In the literature, it has been assumed that the bi-crystal is uniform along the cross-section direction. Thus it is reasonable for us to consider only two-dimensional (2D) geometry in this paper. A robust, numerical method is developed in this work that can approximate the dynamics of this physical situation. The method can also be applied to other mixed order curve network problems.

This geometry contains two types of motion. One of them is mean curvature motion for the grain boundary. The other one is surface diffusion for the upper surfaces. More detail about this model is given in [16]. Motion by mean curvature is a second order parabolic evolution law in which the normal velocity of an interface is given

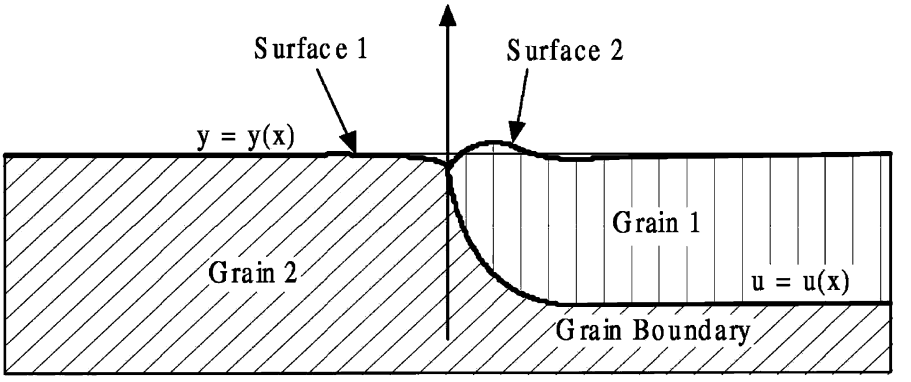

FIGURE 1. The quarter loop bi-crystal geometry.

by

$$V_c = A\kappa. \tag{1}$$

Here, V_c denotes the velocity in the normal direction, κ stands for the mean curvature and A is a physical constant. Surface diffusion is a fourth-order parabolic evolution law, first proposed by Mullins [21] to model the curvature-driven diffusion on the surface of a crystal. With surface diffusion, the normal velocity of an interface is proportional to the surface Laplacian of mean curvature. In two dimensions, the normal velocity is given by

$$V_d = -B\kappa_{ss}. \tag{2}$$

Here, s is arc length parametrisation and B is a physical constant. It is shown in an appendix to this paper that it is possible to take both A and B as one by rescaling time and space.

Surface diffusion is an intrinsically difficult problem to solve numerically even in two dimensions [8, 9, 25]. It is stiff due to the fourth order derivatives such that an explicit time-stepping strategy requires very small time steps. Moreover, owing to the lack of a maximum principle, a curve may self-intersect during its evolution. To handle problems with changing topology due to self intersection, level set methods are typically used, and [25] describes a level set method for curves that move with surface diffusion. However, it is not possible to handle the curves with mixed velocity type and junction conditions of the quarter loop problem in a level set method. Therefore, we have turned to a formulation that involves curve tracking. The formulations in this paper will be proposed in parametrised form.

Several contributions have been made to the study of numerical methods for curvature-driven interface motion problems [4, 7, 9, 20, 25, 33]. For an overview we refer to [10]. In [2, 12], the authors presented formulations allowing only normal direction evolution and therefor redistribution of grid points in the tangential direction was needed to avoid coalescence. The importance of nontrivial tangential velocity has been emphasised and utilised in [7, 20]. In [7], the authors developed a parabolic formulation and utilised its smoothing property to adjust grid points. Another approach for uniform grid distribution is proposed by Mikula and Sevcovic in [20]. They explicitly introduced a

https://doi.org/10.1017/S0956792508007390 Published online by Cambridge University Press

tangential velocity function into the formulation and derived an evolution partial differentiation equation (PDE) to move the points tangentially such that a uniform grid was maintained. Variational formulations were also developed to describe curvature-driven motion and solved by finite element method, for example [27–29] and more recently [3].

The analysis and simulation of the mixed order has been considered in different contexts. In many cases, linearised or model problems are considered as in [30–32]. In other cases, steady state or travelling wave solutions are considered [15–19]. Despite this continued experimental and mathematical interest in the mixed order problem (see also [11, 13, 21]), numerical methods that describe the general, nonlinear, time-dependent evolution of this phenomena had not been developed. In this paper, we contribute a robust numerical method using a finite difference discretisation. The travelling wave solutions for the mixed order problem in [17] are used to verify numerical convergence in this paper. Our computations give some evidence that these travelling waves are stable even to large perturbations. Our method maintains uniform distribution of grid points in arc length without redistribution by interpolation or using an evolution equation for the tangential velocity. Instead, we use an algebraic equation to adjust the position of grid points. This approach does not depend on the type of the motion and therefore the same approach for both the curvature motion and surface diffusion can be used.

Other authors [3] recently and independently considered a similar numerical approach to the type of curve networks we consider here. Their method is based on a variational formulation of the problem and they used a finite element method to approximate it. Careful consideration of their formulation shows that in the semi-discrete case (time continuous) their method leads to uniform distribution of grid points in a manner similar to our approach. However, this exact discrete property is lost in their fully discrete (space and time) scheme but retained in ours. In addition our method is much easier to implement, allowing modifications to the junction conditions and normal motion in a straight-forward way. Neither their method nor ours is particularly amenable to computations in three dimensions (3D) in the situations of interest where complex topological changes occur. Great success has been obtained using thresholding methods for curvature-driven networks in 3D [23]. Some recent work on networks with higher order motion has been done [24]. However, there are difficult unanswered questions on how to implement these techniques for mixed order problems.

The outline of this paper is as follows. In Section 2, equations are derived for the motion by mean curvature and the motion by surface diffusion. The PDEs for the normal motion are augmented by algebraic conditions that the parametrisation be scaled arc length. Our formulation is thus a partial differential algebraic equation (PDAE) system. The boundary conditions including the triple junction conditions and approximate far-field boundary conditions are also discussed. In Section 3, the well-posedness for a linear, PDAE system that is closely related to the full nonlinear problem is analysed. Both the problem and our formulation are shown to be well-posed in this setting. In Section 4, we discuss the numerical details including discretisation and time stepping. A convergence study to an exact travelling wave solution is given. In Section 5, we use our method on two more examples of interest: the Sun–Bauer geometry and grain growth in a thin film array.

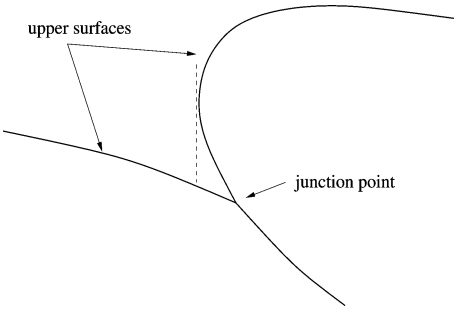

FIGURE 2. An example when one of the surfaces is not single-valued.

2 The formulation

In this section, we derive a PDAE system to model the coupled motion. It is a new formulation of the quarter loop problem. Other formulations of the problem are presented in detail in [16, 17, 19]. For the coupled grain boundary motion, the function $y(x)$ which represents the exterior surface may not be single-valued as shown in Figure 2. This phenomena is physically reasonable [15, 18]. For this reason, we use parametrised curves to describe the interfaces. Here and throughout this paper we use $X = (u(\cdot), v(\cdot))$ to represent a parametrised curve with $u(\cdot)$ and $v(\cdot)$ being the coordinates. The arc length parameter is denoted by s. In the method presented below, σ will denote a parameter that is scaled arc length, where the scaling can be different for each curve and where σ is in the fixed interval [0, 1] with $\sigma = 0$ the junction and $\sigma = 1$ the edge of the computational domain. The vectors τ and n stand for unit tangential direction and unit normal direction, respectively. κ stands for curvature.

2.1 Motion by mean curvature

The basic evolution law (1) should be satisfied, i.e.,

$$X_t \cdot n - \kappa = 0. \tag{3}$$

However, this leaves the tangential velocity arbitrary. In [7], the problem was extended to be parabolic in both components in a convenient way. A discretisation of this model was applied successfully to curve networks with junctions: the tangential parabolicity makes the parametrisation more uniform in time. The natural extension of this idea to surface diffusion (discussed below) would make the tangential components of that motion fourth order parabolic as considered in [13]. This approach leads to a scheme with parameters in the tangential parabolicity that need to be chosen carefully to keep a monotone parametrisation in a numerical approximation. Details of this approach as well as an approximation in Cartesian formulation can be found in the archival report [22].

Much better numerical performance is achieved using the following approach. Equation (3) is augmented by a condition that directly imposes uniform grid spacing:

$$|X_\sigma|_\sigma = 0. \tag{4}$$

https://doi.org/10.1017/S0956792508007390 Published online by Cambridge University Press

Note that

$$|X_\sigma|_\sigma = (\sqrt{X_\sigma \cdot X_\sigma})_\sigma = \frac{X_\sigma \cdot X_{\sigma\sigma}}{|X_\sigma|}.$$

so (4) can be replaced by

$$X_\sigma \cdot X_{\sigma\sigma} = 0. \tag{5}$$

The idea of maintaining equally spaced grid points on a curve has been considered in several other works [14, 20]. Our problem is simpler than some described in [14] in that it is not necessary to keep track of material points on the curves. The idea of applying (5) to enforce an equi-spaced parametrisation appears to be a new idea. In previous work, particular choices of tangential velocities were used that caused the parametrisation to move towards an equi-spaced parametrisation.

We have

$$\begin{aligned} X_s &= \tau \\ n &= \tau^\perp \\ X_{ss} &= \kappa n. \end{aligned}$$

Thus, κ in (3) above can be replaced by the expression

$$\kappa = \frac{X_{\sigma\sigma}}{|X_\sigma|^3} \cdot X_\sigma^\perp \tag{6}$$

involving σ derivatives.

2.2 Motion by surface diffusion

In a similar way we derive the PDAEs for the motion by surface diffusion,

$$\begin{aligned} X_t \cdot n + \kappa_{ss} &= 0 \\ X_\sigma \cdot X_{\sigma\sigma} &= 0. \end{aligned} \tag{7}$$

Using the fact that σ will be scaled arc length, this leads us to the expression

$$\kappa_{ss} = \frac{\kappa_{\sigma\sigma}}{|X_\sigma|^2} \tag{8}$$

to be used in (7), where κ is computed from (6).

2.3 The system

We use superscripts to denote the three curves, 1 for the grain boundary, 2 for the upper left surface and 3 for the upper right surface as shown in Figure 3. The full PDAE system for the coupled motion is

$$\left.\begin{aligned} X_t^1 \cdot n - \kappa &= 0 & \\ X_t^i \cdot n + \kappa_{ss} &= 0 & i = 2,3 \\ X_\sigma^i \cdot X_{\sigma\sigma}^i &= 0 & i = 1,2,3 \end{aligned}\right\}. \tag{9}$$

https://doi.org/10.1017/S0956792508007390 Published online by Cambridge University Press

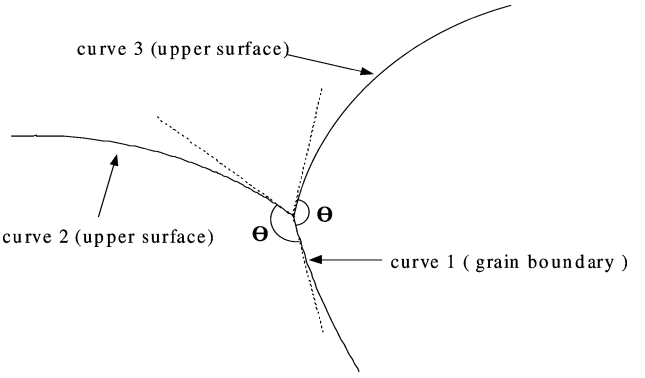

FIGURE 3. Sketch of the grain boundary groove showing the curve numbering.

This is an index-1 PDAE system. Usually an index-1 DAE can be handled without any numerical difficulties [1], and that is our experience with discretisations of this system.

2.4 Boundary conditions

The grain boundary and the two upper surfaces meet together at one end ($\sigma = 0$) which is referred as triple junction. The other end of the three curves tends to infinity in the quarter loop geometry. For numerical reasons, we compute this problem in a bounded domain. This domain is chosen large enough such that it can simulate the motion accurately at least for a short time. This restriction is reasonable since the curves are asymptotically flat for the parts far away from the triple junction. Computations presented later in this paper are constrained in a finite but 'large enough' domain and the curves are parametrised with $\sigma \in [0, 1]$. At $\sigma = 1$ the three curves meet the artificial domain boundary separately.

2.4.1 *Triple junction conditions at* $\sigma = 0$

We first discuss the boundary conditions at the triple junction, see Figure 3. The three curves should have common coordinates at $\sigma = 0$, i.e.,

$$X^1(0,t) = X^2(0,t) = X^3(0,t). \tag{10}$$

A balance of surface tensions (Young's law) gives two angle conditions:

$$\frac{X^1_\sigma}{|X^1_\sigma|} \cdot \frac{X^i_\sigma}{|X^i_\sigma|} = \cos\theta = \cos\left(\frac{\pi}{2} + \arcsin\frac{m}{2}\right) \qquad i = 2, 3, \tag{11}$$

where θ denotes the angle between the grain boundary and the exterior surfaces and $m = \gamma_{\text{grain}}/\gamma_{\text{exterior}}$ is a constant measuring the relative surface tensions γ between them. The continuity of the surface chemical potentials implies that

$$\kappa^2 = -\kappa^3 \tag{12}$$

https://doi.org/10.1017/S0956792508007390 Published online by Cambridge University Press

and the balance of mass flux implies that

$$\kappa_s^2 = \kappa_s^3, \tag{13}$$

where the expression for κ_s is obtained by taking the derivative of the expression of κ directly. We must be careful about condition (12) which specifies that the two upper surfaces have the same convexity. Since σ has opposite directions for the two curves, the odd derivatives will have opposite signs when computed by parametric form. Thus we should put a minus sign for (12) and keep the same sign for (13).

2.4.2 *Boundary conditions at* $\sigma = 1$

At the other ends of the curves we put several artificial conditions such that they do not move during evolution and stay 'flat'. The following conditions are imposed at $\sigma = 1$,

$$\begin{aligned} X_t^i(1,t) &= \mathbf{0} \qquad \text{for } i = 1,2,3 \\ X_{\sigma\sigma}^i(1,t) &= \mathbf{0} \qquad \text{for } i = 2,3. \end{aligned}$$

3 Well-posedness for the PDAE system

In this section, we analyse the well-posedness of a linear model of the system proposed above. We linearise around fixed straight line solutions and get a system that has the same highest order behaviour as the original problem near the junction. The analysis here gives results that match those that more complicated nonlinear analysis gives, where such analysis exists [6, 13]. Therefore, we believe the results of the analysis should apply to the full nonlinear problem. In [6], three curves moving with curvature motion meeting at a junction are analysed. In [13], three curves undergoing surface diffusion meeting at a junction are analysed. There is a gap in the theory for the quarter loop problem, which is of mixed order, for which the underlying theoretical estimates for the equal order problems in [26] are not available. The analysis below corresponds to the first step in such estimates.

3.1 Linearisation of the system

To linearise the system we consider a perturbation expansion around the tangential direction at the triple junction for each curve, i.e.,

$$\begin{aligned} X^1 &= d_1\sigma + \epsilon\bar{X}^1 + O(\epsilon^2) \\ X^2 &= d_2\sigma + \epsilon\bar{X}^2 + O(\epsilon^2) \\ X^3 &= d_3\sigma + \epsilon\bar{X}^3 + O(\epsilon^2), \end{aligned}$$

where $d_i = (d_{i1}, d_{i2})$ are constant vectors standing for the unit tangential direction. Substituting the above forms into (9), keeping only the leading order terms and dropping the

https://doi.org/10.1017/S0956792508007390 Published online by Cambridge University Press

bar superscript results in the linear system:

$$\left.\begin{array}{ll} X_t^1 \cdot d_1^\perp = X_{\sigma\sigma}^1 \cdot d_1^\perp & \\ X_t^i \cdot d_i^\perp = -X_{\sigma\sigma\sigma}^i \cdot d_i^\perp & i = 2,3 \\ d_i \cdot X_{\sigma\sigma}^i = 0 & i = 1,2,3 \end{array}\right\}. \tag{14}$$

The linearisation of the triple junction conditions is given below:
Common point at $\sigma = 0$:

$$X^1 = X^2 = X^3 \tag{15}$$

Angle conditions:

$$d_1 \cdot X_\sigma^i + d_i \cdot X_\sigma^1 - (d_1 \cdot d_i)\left(d_1 \cdot X_\sigma^1 + d_i \cdot X_\sigma^i\right) = 0 \qquad i = 2,3 \tag{16}$$

Continuity of surface chemical potential:

$$X_{\sigma\sigma}^2 \cdot d_2^\perp = -X_{\sigma\sigma}^3 \cdot d_3^\perp \tag{17}$$

Balance of mass flux:

$$X_{\sigma\sigma\sigma}^2 \cdot d_2^\perp = X_{\sigma\sigma\sigma}^3 \cdot d_3^\perp. \tag{18}$$

Without changing the well-posedness of the problem we specify one of the tangential directions, say $d_1 = (0,-1)^T$. Further we assume

$$\theta \in \left(\frac{\pi}{2}, \pi\right) \tag{19}$$

so that $d_{i,1}, d_{i,2} \neq 0$ for $i = 2,3$. The linearised system (14) has solution in the form

$$\left.\begin{array}{l} u_1 = A_{11} e^{-\sqrt{s}\sigma} \\ v_1 = B_{11} \\ u_2 = A_{21} e^{\lambda_1 \sigma} + B_{21} e^{\lambda_2 \sigma} + C_{21} \\ v_2 = -k_2\left(A_{22} e^{\lambda_1 \sigma} + B_{22} e^{\lambda_2 \sigma}\right) + \frac{1}{k_2} C_{21} \\ u_3 = A_{31} e^{\lambda_1 \sigma} + B_{31} e^{\lambda_2 \sigma} + C_{31} \\ v_3 = -k_3\left(A_{32} e^{\lambda_1 \sigma} + B_{32} e^{\lambda_2 \sigma}\right) + \frac{1}{k_3} C_{31} \end{array}\right\}. \tag{20}$$

The variables above stand for their Laplace transforms and s temporarily stands for the Laplace transform variable. The term $k_i = d_{i1}/d_{i2}$ is a constant and

$$\lambda_1 = \left(-\frac{\sqrt{2}}{2} + \frac{\sqrt{2}}{2} i\right) \sqrt[4]{s},$$

$$\lambda_2 = \left(-\frac{\sqrt{2}}{2} - \frac{\sqrt{2}}{2} i\right) \sqrt[4]{s}.$$

https://doi.org/10.1017/S0956792508007390 Published online by Cambridge University Press

In the expressions above, we consider $Re(s) > 0$ and the roots of s are chosen such that

$$|\arg(\sqrt{s})| < \frac{\pi}{2}, \qquad \left|\arg\left(s^{1/4}\right)\right| < \frac{\pi}{4} \tag{21}$$

When these solutions are applied to the boundary conditions (15)–(18), an 8×8 matrix M is obtained. The determinant of M can be computed directly:

$$|M| = \frac{s^{7/4}\left(4\sqrt{2}\sin(2\theta) - 16s^{1/4}\sin\theta\right)}{\cos^4\theta}. \tag{22}$$

The problem will be well-posed with at most algebraic growth in time provided that this determinant is nonzero for any s with $Re(s) > 0$. Under the conditions in (19), we see that (22) can only be zero when $s^{1/4}$ is negative real, violating (21). In summary, the problem is well-posed as long as all angles at the junction are less than π. The marginal case $\theta = \pi/2$, excluded above, can also be shown to be well-posed.

4 Numerical discretisation

In this section, we present the discretisation of the PDAE system (9) and junction conditions (10)–(13). The basic approach is to use a staggered grid in σ and we shall denote the approximations by capital letters with subscripts, i.e., $X_j(t) \approx X((j-1/2)h, t) = (u((j-1/2)h, t), v((j-1/2)h, t))$ where h is the grid spacing and $N = 1/h$ is the number of interior grid points for $\sigma \in [0, 1]$.

Let D_k denotes the second order centred approximation of the kth derivative, i.e.,

$$D_1 X_j = (X_{j+1} - X_{j-1})/2h$$
$$D_2 X_j = (X_{j+1} + X_{j-1} - 2X_j)/h^2$$

and let D_+ and $\mathscr{F}$ denote forward differencing and forward averaging, respectively,

$$D_+ X_j = (X_{j+1} - X_j)/h,$$
$$\mathscr{F} X_j = (X_{j+1} + X_j)/2.$$

Using these standard differences, κ in (6) and then the surface diffusion term κ_{ss} in (8) can be computed. Note that the ghost values $X_0^1, X_0^2, X_0^3, \kappa_0^2$ and κ_0^3 are needed to complete the stencils of these discrete equations, see Figure 4. These eight values can be related to interior values using the eight junction conditions (10)–(13) as shown below. The discretisation at the junction is somewhat subtle. Instead of using two ghost points for each fourth order surface diffusion problem we use only one ghost point ($X^i(0)$) plus another ghost value (κ_0^i) indicating the curvature at the ghost point. Other approaches [22] may require additional tangential conditions at the triple junction.

4.1 Junction conditions

Condition (10) is approximated by

$$\mathscr{F} X_0^1 = \mathscr{F} X_0^2 = \mathscr{F} X_0^3. \tag{23}$$

https://doi.org/10.1017/S0956792508007390 Published online by Cambridge University Press

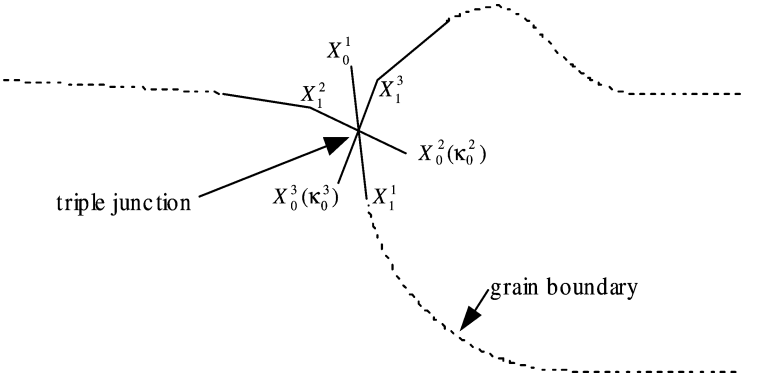

FIGURE 4. Sketch of the ghost values at the triple junction.

The angle conditions (11) are approximated by

$$\frac{D_+X_0^1}{|D_+X_0^1|} \cdot \frac{D_+X_0^i}{|D_+X_0^i|} = \cos\theta \qquad i = 2, 3.$$

Conditions (12) and (13) are approximated by

$$\mathscr{F}\kappa_0^2 = -\mathscr{F}\kappa_0^3$$
$$\frac{D_+\kappa_0^2}{|D_+X_0^2|} = \frac{D_+\kappa_0^3}{|D_+X_0^3|}.$$

The discretisation of the artificial conditions at $\sigma = 1$ is straightforward.

4.2 Time stepping

In order to avoid the excessively small time steps due to the stiffness of the surface diffusion term, we use implicit time stepping. For simplicity we use backward Euler method. It is found computationally that spatial errors dominate temporal errors. Since the three curves are strongly coupled by the junction, we solve for interior and ghost points simultaneously. The nonlinear system is solved by Newton's method.

4.3 Numerical results

We compare the numerical results to an exact travelling wave solution [17]. An example is shown in Figure 5. Notice the uniformity of the grid points enforced by our formulation. A numerical convergence study is shown in Table 1. The convergence rates shown in Table 1 are close to 2 as expected.

Without difficulty we can apply this scheme to the case when the surface curve is not a single-valued function as shown in Figure 6.

Another example is shown in Figure 7. Here, a large perturbation to a travelling wave solution is given. The travelling wave structure redevelops after some time. This and other runs conducted with similar behaviour indicate the 2D stability of these travelling wave solutions.

https://doi.org/10.1017/S0956792508007390 Published online by Cambridge University Press

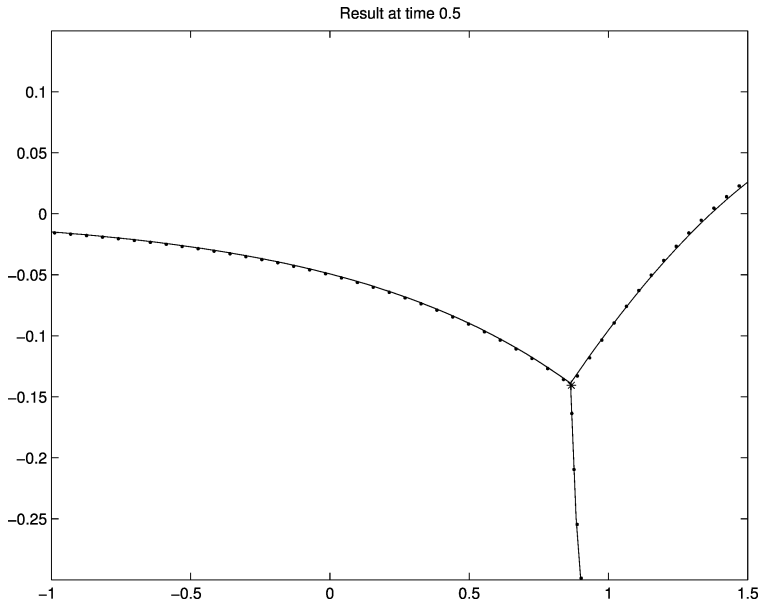

FIGURE 5. Comparison of the numerical solution to the exact travelling wave, zoomed in near triple junction. Dotted line: numerical solution; solid line: travelling wave solution; time step size: $\Delta t = 0.01$.

Table 1. *Estimated errors and convergence rates for PDAE formulation with* $m = 0.5$. *Errors are evaluated at* $t = 0.02$

dt	Δs	L_2 norm	Rate	L_∞ norm	Rate
	0.2	2.7837e-04		1.8996e-03	
$dt = 0.01\Delta s^2$	0.1	7.2717e-05	1.9366	5.4444e-04	1.8029
	0.05	1.8732e-05	1.9568	1.4732e-04	1.8858

5 More examples

In this section, we consider two more examples, the Sun–Bauer geometry [19, 31, 32] and the grain growth in a thin film array [5, 30]. Both examples preserve the complexity of the the coupled motion but are considered in different contexts in which travelling wave solutions are not available. Previous studies considered linearised or approximate problems. Our method is able to accurately compute the full nonlinear problem.

In the Sun–Bauer geometry, an initially straight grain boundary attaches to the exterior surface with an inclination angle β as shown in Figure 8. After annealing, the grain boundary migrates to the right with inclination angle α at the groove root. The same junction conditions as in the quarter loop geometry are applied. In [19, 31, 32], the authors studied the mobility of grain boundary under different inclination angle β. They assumed, the grain boundary migrates at a constant speed which is measured in an experiment and then iterates linearised surface diffusion and grain boundary motions alternately. They considered the asymptotic behaviour of the grain boundary when β is

https://doi.org/10.1017/S0956792508007390 Published online by Cambridge University Press

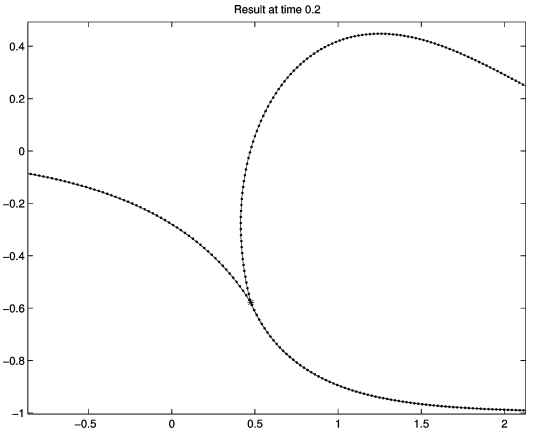

FIGURE 6. Plot of the results for scheme with $m = 1.96$ which has non-single-valued upper surface. Dotted line: numerical result; solid line: travelling wave solution.

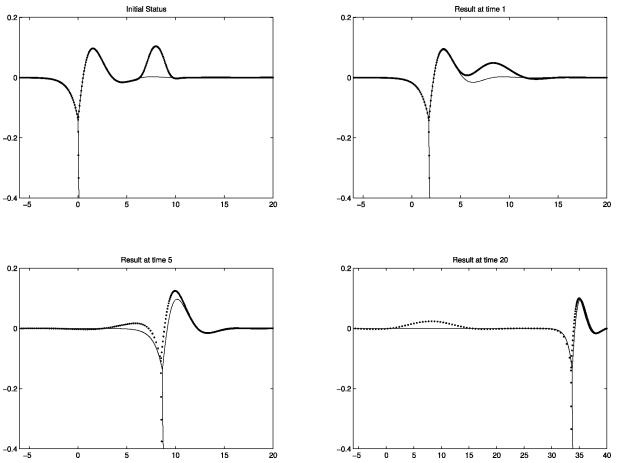

FIGURE 7. Results for initial data that is a perturbation of a travelling wave.

small and drew the conclusion that the coupled motion can be separated into two time regimes. In Regime I, the grain boundary turns vertically at the groove root. In Regime II, the turning relaxes following two different paths depending on the value of γ/β where $\gamma = 2\arcsin(\frac{m}{2})$ is the supplementary dihedral angle between the exterior surfaces. If $\beta < \gamma/6$, the grain boundary root moves continuously away from the initial position, but the grain boundary tries to remain straight. For $\beta > \gamma/6$, the grain boundary bends towards the free surface to be inclined with angle $\gamma/6$ at the groove root.

Figures 9 and 10 show the numerical results solved from our coupled nonlinear formulation with different inclination angle β. The simulations start with a straight line attached to a horizontal surface. The relative surface tension is $m = 0.5$ and therefore $\gamma/6 = 0.083$. Figure 9 shows the results with $\beta = 0.05$ and Figure 10 uses $\beta = 0.9$. The grain boundary turns almost perpendicular (α is small) at the beginning and then follows two different paths as described in [19, 31, 32]. For $\beta = 0.05 < \gamma/6$, inclination angle α

https://doi.org/10.1017/S0956792508007390 Published online by Cambridge University Press

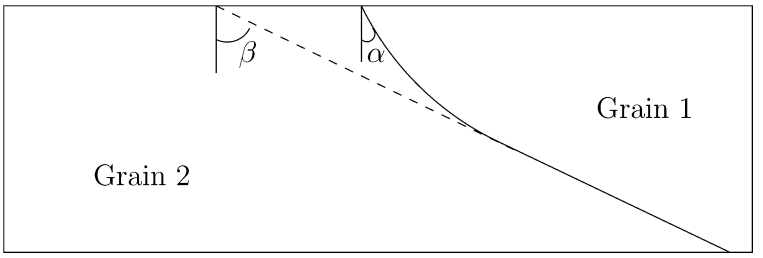

FIGURE 8. The Sun–Bauer geometry.

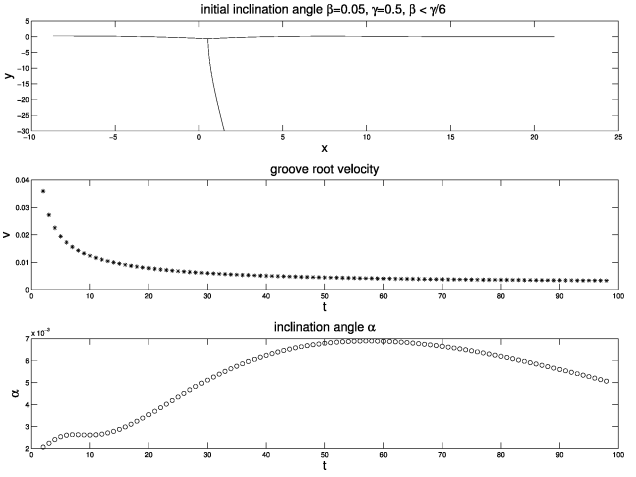

FIGURE 9. Sun–Bauer geometry simulation with $\beta < \gamma/6$. Top: the groove and grain boundary profile; middle: groove velocity versus time; bottom: inclination angle versus time.

keeps being small. For $\beta = 0.9 > \gamma/6$, α begins to increase and approaches to a value (roughly 0.078) that is smaller than but roughly comparable to the value $\gamma/6$ in the linear, approximate theory [19, 31, 32]. The velocity of groove root is also shown as a function of time. It is not constant but the acceleration is small especially after some time of evolution. Our accurate nonlinear simulations of the full model show that the predictions of the earlier work are approximately valid.

The second example is about the grain growth in a thin film array. In [30], it is predicted that film breakup occurs when grain sizes are larger than the film thickness. They simulated the case when breakup occurs using an approximate linear system, assuming the surface and the boundary deviate slightly from their inclinations. We employed our formulation to compute the evolution of a periodic array in a 2D film where breakup occurs. The computation starts with grain boundaries perpendicular to exterior surface. The qualitative behaviour in our simulation shown in Figure 11 is similar to the results in [30]. However, there are certain geometric anomalies in the earlier work (angles at triple junctions are not matched accurately) from approximations made in their model that are computed correctly by our approach.

https://doi.org/10.1017/S0956792508007390 Published online by Cambridge University Press

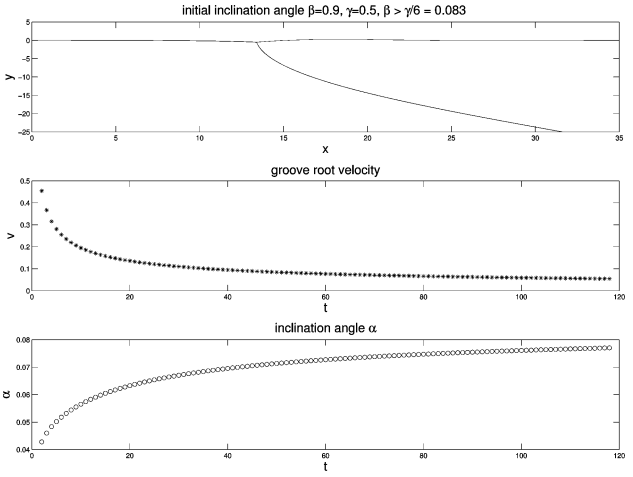

FIGURE 10. Sun–Bauer geometry simulation with $\beta > \gamma/6$. Top: the groove and grain boundary profile; middle: groove velocity versus time; bottom: inclination angle versus time.

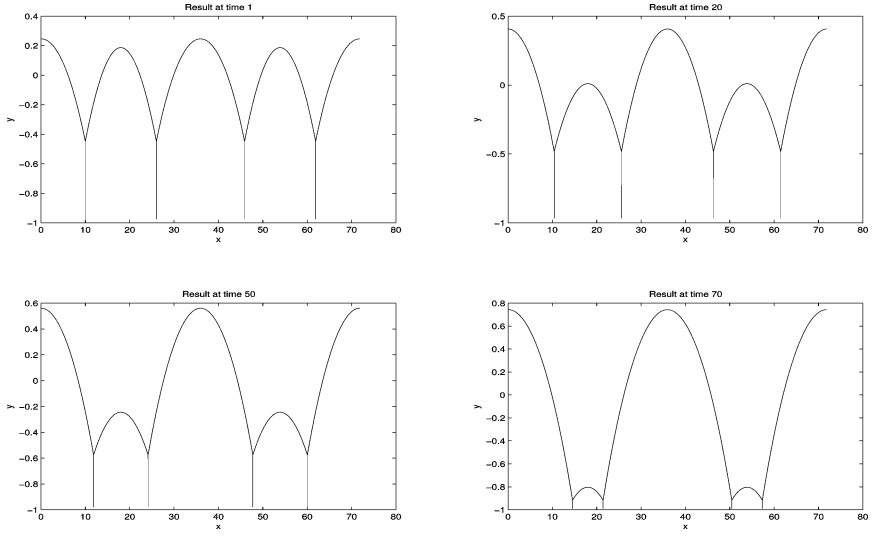

FIGURE 11. The evolution of film morphology during breakup.

6 Conclusion

In this work, we proposed a new formulation to describe coupled surface and grain boundary motion. This formulation is well-posed (shown in a reduced, linear setting) and easy to implement numerically with finite differences. The numerical method is shown to converge to an exact solution with expected accuracy. It was applied to several cases of physical interest, giving more accurate solutions than previous studies. An attractive feature of the scheme is that grid points on each curve are equi-spaced. This maintains uniform resolution and allows for convenient global regridding when necessary. This could be necessary as curves in a network expand or shrink.

https://doi.org/10.1017/S0956792508007390 Published online by Cambridge University Press

This scheme can also be used to efficiently simulate the motion of a curve that involves only mean curvature motion or surface diffusion as shown in [22]. It is more accurate than the scheme proposed in [7] for curvature motion networks. It is the scheme with the best overall performance of several finite difference approaches to this problem [22].

An avenue that has received no attention in the literature is the behaviour of this problem in 3D. In future work, the authors intend to pursue basic questions such as the stability of the travelling waves found in [17] to 2D and then 3D perturbations. Some evidence of the stability of travelling waves to 2D perturbations is given by the computations in this work.

Acknowledgements

The authors would like to thank Amy Novick-Cohen for helpful conversations on this problem, its background and related work. This research was supported by an NSERC Canada grant.

Appendix. Scaling the motion laws

The original curvature motion and surface diffusion are given as

$$\left.\begin{aligned} X_t \cdot n &= A\kappa \\ Y_t \cdot n &= -B\kappa_{ss} \end{aligned}\right\}. \tag{24}$$

We show here that both A and B can be made unity by rescaling time and space.

We scale time by

$$\tilde{t} = Tt.$$

The spatial variable X, Y are scaled

$$\tilde{X} = RX, \quad \tilde{Y} = RY.$$

We can easily verify that

$$\tilde{s} = Rs,$$

where $\tilde{s}$ is the arc length in the new system. It also follows that

$$\tilde{X}_{\tilde{s}} = X_s, \quad \tilde{Y}_{\tilde{s}} = Y_s, \quad \tilde{\kappa} = \frac{1}{R}\kappa, \quad \tilde{\kappa}_{\tilde{s}\tilde{s}} = \frac{1}{R^3}\kappa_{ss}.$$

Now equation (24) becomes

$$\left.\begin{aligned} \tilde{X}_{\tilde{t}} \cdot n &= \tfrac{AR^2}{T}\tilde{\kappa} \\ \tilde{Y}_{\tilde{t}} \cdot n &= -\tfrac{BR^4}{T}\tilde{\kappa}_{\tilde{s}\tilde{s}} \end{aligned}\right\}. \tag{25}$$

Here we use the same notation n since the normal direction does not change. If we choose

$$R = \sqrt{\frac{A}{B}}, \quad T = \frac{A^2}{B}$$

https://doi.org/10.1017/S0956792508007390 Published online by Cambridge University Press

then equation (25) becomes

$$\tilde{X}_{\tilde{t}} \cdot n = \tilde{\kappa}$$
$$\tilde{Y}_{\tilde{t}} \cdot n = -\tilde{\kappa}_{\tilde{s}\tilde{s}}.$$

This completes the normalisation of coefficients A and B. Note that in [17], the authors retain the ratio A/B in their equations. They use the remaining degree of freedom to normalise the distance between the grain boundary and the upper surface far from the junction in their travelling wave solutions.

References

[1] Ascher, U. M. & Petzold, L. R. (1998) Computer methods for ordinary differential equations and differential-algebraic equations. *SIAM*. Philadelphia, PA.

[2] Bansch, E., Morin, P. & Nochetto, R. H. (2005) A finite element method for surface diffusion: The parametric case. *J. Comput. Phys.* **203**(1), 321–343.

[3] Barrett, J. W., Garckeb, H. & Nurnberg, R. (2007) On the variational approximation of combined second and fourth order geometric evolution equations. *SIAM J. Sci. Comput.* **29**(3), 1006–1041.

[4] Barrett, J. W., Garckeb, H. & Nurnberg, R. (2007) A parametric finite element method for fourth order geometric evolution equations. *J. Comput. Phys.* **222**, 441–467.

[5] Brokman, A., Kris, R., Mullins, W. W. & Vilenkin, A. J. (1995) Analysis of boundary motion in thin films. *Scr. Metall. Mater.* **32**, 1341–1346.

[6] Bronsard, L. & Reitich, F. (1993) On three-phase boundary motion and the singular limit of a vector-valued Ginzburg–Landau equation. *Arch. Ration. Mech. Anal.* **124**(4), 355–379.

[7] Bronsard, L. & Wetton, B. T. R. (1995) A numerical method for tracking curve networks moving with curvature motion. *J. Comput. Phys.* **120**, 66–87.

[8] Cahn, J. & Taylor, J. (1994) Overview 113: Surface motion by surface diffusion. *Acta Metall. Mater.* **42**, 1045–1063.

[9] David, L. C. & Sethian, J. A. (1999) Motion by intrinsic Laplacian of curvature. *Interfaces Free Boundaries* **1**, 1–18.

[10] Deckelnick, K., Dziuk, G. & Elliott, C. M. (2005) Computation of geometric partial differential equations and mean curvature flow. *Acta Numerica* **14**, 139–232.

[11] Dunn, C. G. & Sharp, M. (1952) Secondary recrystallization texture in Copper. *Trans AIME* **194**, 42–43.

[12] Dziuk, G., Kuwert, E. & Schatzle, R. (2002) Evolution of elastic curves in $\mathbb{R}^n$: Existence and computation. *SIAM J. Math. Anal.* **33**, 1228–1245.

[13] Garcke, H. & Novick-Cohen, A. (2000) A singular limit for a system of degenerate cahn-hilliard equations. *Adv. Differ. Equs.* **5**, 401–434.

[14] Hou, T. Y., Lowengrub, J. S. & Shelley, M. J. (2001) Boundary integral methods for multicomponent fluids and multiphase materials. *JCP* **169**, 302–362.

[15] Kanel, J. & Novick-Cohen, A. (2004) Coupled surface and grain boundary motion: Nonclassical traveling wave solutions. *Adv. Differ. Equs.* **9**, 299–327.

[16] Kanel, J., Novick-Cohen, A. & Vilenkin, A. (2003) A traveling wave solution for coupled surface and grain boundary motion. *Acta Mater.* **51**, 1981–1989.

[17] Kanel, J., Novick-Cohen, A. & Vilenkin, A. (2004) Coupled surface and grain boundary motion: A travelling wave solution. *Nonlinear Anal.* **59**, 1267–1292.

[18] Kanel, J., Novick-Cohen, A. & Vilenkin, A. (2005) A numerical study of grain boundary motion in bicrystals. *Acta Mater.* **53**, 227–235.

[19] Min, D. & Wong, H. (2004) A model of migrating grain-boundary grooves with application to two mobility-measurement methods. *Acta Mater.* **50**, 5155–5169.
[20] Mikula, K. & Sevcovic, D. (2004) Computational and qualitative aspects of curves driven by curvature and external force. *Comput. Vis. Sci.* **6**, 211–225.
[21] Mullins, W. W. (1957) Theory of thermal grooving. *J. Appl. Phys.* **28**, 333–339.
[22] Pan, Z. & Wetton, B. Numerical methods for coupled surface and grain boundary motion, arXiv report math.NA/0702503. URL: http://arxiv.org/. Submitted 2007, last updated February 16, 2007.
[23] Ruuth, S. J. (1998) Efficient algorithms for diffusion-generated motion by mean curvature. *J. Comput. Phys.* **144**, 603–625.
[24] Esedoglu, S. & Tsai, R., Threshold dynamics for high order geometric motions. To appear in *Interfaces Free Boundaries.*
[25] Smereka, P. (2003) Semi-Implicit level set methods for curvature and surface diffusion motion. *J. Sci. Comput.* **19**(1–3), 439–456.
[26] Solonnikov, V. A. (1965) Boundary value problems in physics, In: Proceedings of the Steklov Institute of Mathematics, Vol. 83, pp. 487–491.
[27] Sun, B., Suo, Z. & Yang, W. (1997) A finite element method for simulating interface motion, part I: Migration of phase and grain boundaries. *Acta Mater.* **45**, 1907–1915.
[28] Sun, B. & Suo, Z. (1997) A finite element method for simulating interface motion, part II: Large shape changes due to surface diffusion. *Acta Mater.* **45**, 4953–4962.
[29] Suo, Z. (1997) Motions of microscopic surfaces in materials. *Adv. Appl. Mech.* **33**, 193–294.
[30] Vilenkin, A. J. & Kris, R. (1997) Breakup and grain growth in thin-film array. *J. Appl. Phys.* **81**, 238–245.
[31] Zhang, H. & Wong, H. (2002) Coupled grooving and migration of inclined grain boundaries: Regime I. *Acta Mater.* **50**, 1983–1994.
[32] Zhang, H. & Wong, H. (2002) Coupled grooving and migration of inclined grain boundaries: Regime II. *Acta Mater.* **50**, 1995–2012.
[33] Zhang, W. & Schneibel, J. H. (1995) Numerical Simulation of grain-boundary grooving by surface diffusion. *Comput. Mater. Sci.* **3**, 347–358.